THE JOURNAL OF PHYSICAL CHEMISTRY B

Article

pubs.acs.org/JPCB

Dynamics of Water in Gemini Surfactant-Based Lyotropic Liquid Crystals

Jesse G. McDaniel, Sriteja Mantha, and Arun Yethiraj*

Department of Chemistry, University of Wisconsin, Madison, Wisconsin 53706, United States

Supporting Information

ABSTRACT: The dynamics of water confined to nanometer-sized domains is important in a variety of applications ranging from proton exchange membranes to crowding effects in biophysics. In this work, we study the dynamics of water in gemini surfactant-based lyotropic liquid crystals (LLCs) using molecular dynamics simulations. These systems have well characterized morphologies, for example, hexagonal, gyroid, and lamellar, and the surfaces of the confining regions can be controlled by modifying the headgroup of the surfactants. This allows one to study the effect of topology, functionalization, and interfacial curvature on the dynamics of confined water. Through analysis of the translational diffusion and rotational relaxation, we conclude that the hydration level and resulting confinement length scale is the predominate determiner of the rates of water dynamics, and other effects, namely, surface functionality and curvature, are largely secondary. This novel analysis of the water dynamics in these LLC systems provides an important comparison for previous studies of water dynamics in lipid bilayers and reverse micelles.

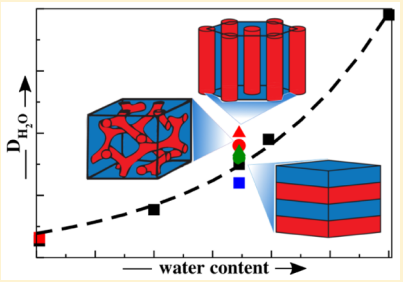

1. INTRODUCTION

Many biological and chemical systems are composed of water in various states of nanoconfinement. For example, phospholipid membranes,[1] reverse micelles,[2] nanotubes,[3] silica nanopores,[4] Nafion membranes,[5] and surfactant-based lyotropic liquid crystals (LLCs)[6] all exhibit hydration levels at which water is confined to nanometer-sized regions. In these systems, the dynamics of water is dramatically altered relative to the bulk,[7,8] affecting nearly all other kinetic phenomena, including small-molecule and ion transport. A fundamental knowledge of how confinement affects water dynamics is therefore essential for understanding many important biological processes as well as materials applications.

Of particular interest is the extent to which the specific confinement topology affects the water dynamics. For example, one might expect that the curvature of the confining region is important, with negative curvature (water inside reverse micelles) being more restrictive than flat (water at a lamellar bilayer), or positive curvature (water at a cylinder). Correspondingly, reverse micelles and phospholipid bilayers have served as prototypical systems for studying the dynamics of nanoconfined water, with both experimental[2,9−22] and theoretical studies[23−30] examining the effect of these different confinement topologies. Contradictory conclusions exist as to the influence of the interfacial curvature of the confining surface: Moilanen et al.[18] concluded that differences in interfacial curvature of reverse micelles and lamellar lipid bilayers had a small effect on water dynamics. However, Roy et al.[31] recently reached a very different conclusion, suggesting that differences in curvature of reverse micelles and gyroid-phase LLCs significantly affected water dynamics.

In addition to the curvature, the chemical functionalization of the interface is expected to affect the water dynamics. Indeed it has been shown that the functionalization of the interface dictates the surface structure of water.[32−34] Surface−water hydrogen bonds may have significantly different energies relative to bulk water hydrogen bonds,[2,15,27,35] potentially affecting the water dynamics.[35−40] However, spectroscopic studies of both ionic and nonionic surfactant-based reverse micelles implied that the nature of the interface was of secondary importance for the orientational relaxation of water.[17]

A significant complication in previous studies is the inability to directly isolate the different effects of surface functionality, curvature, and relative hydration level within different confining media. In this work, we investigate the dynamics of water in gemini surfactant-based LLCs.[6,41−48] These are ideal systems because they exhibit a variety of morphologies of different interfacial curvature including lamellar, gyroid, and hexagonal phases.[6] In addition, these phases are modulated by varying the surfactant linker or tail length, headgroup, counterion, temperature, or hydration level.[48,49] To our knowledge, only a handful of studies[31,49,50] have examined the dynamics of water in these systems.

In this work, we systematically isolate the effects of morphology, water content, and surfactant functionality on the water dynamics in gemini surfactant-based LLCs. Using molecular dynamics (MD) simulations, we compare the dynamics of water in three different LLC morphologies,

Received: August 10, 2016
Revised: September 21, 2016
Published: September 26, 2016

DOI: 10.1021/acs.jpcb.6b08087
J. Phys. Chem. B 2016, 120, 10860−10868

hexagonal, gyroid, and lamellar phases, *at identical water content*; this allows direct characterization of the effect of morphology and interfacial curvature on the dynamics at constant hydration level. Additionally, we study both carboxylate and sulfonate surfactant-based LLCs, allowing analysis of the effect of surface functionalization. As a reference, we characterize longer-tail surfactant lamellar phases at varying hydration level. The water dynamics in all of these systems is characterized through the translational diffusion and rotational relaxation.

Our general conclusion is that hydration level and confinement length scale predominately determines rates of water dynamics, and variables such as interfacial curvature and surface functionalization are secondary in importance. Because the water content and confinement length scales of the gemini surfactant-based LLCs are comparable to the analogous parameters of reverse micelles and lipid bilayers, our work provides an important comparison for the large body of research focused on the latter systems. Additionally, we believe that our present study is advantageous in its unequivocal isolation of the distinct effects of interfacial curvature, surface functionalization, and water content. We finally note that the systematic comparison of this work is possible only through computer simulations, because some of the LLCs are metastable and may not be experimentally accessible.

2. METHODS

We study a total of 11 gemini surfactant-based LLCs, composed of different surfactants at different hydration levels; henceforth, the hydration level is denoted by λ, the number of water molecules per surfactant (note that $\lambda/2$ is then the number of water molecules per headgroup). The gemini surfactants, shown in Figure 1, are denoted by "Head-$N_{tail}(N_{link})$", where "Head" is the surfactant headgroup (CO_2^- or SO_3^-), N_{tail} is the number of carbon atoms of the surfactant tails (we consider N_{tail} = 7 or 13), and N_{link} is the number of carbon atoms in the linker (here, N_{link} = 4). All systems are then composed of such surfactants, sodium counterions, and water molecules. Five systems are lamellar phases of CO_2-13(4), at hydration levels λ = 6.1, 10, 12.9, 13.9, and 18. Three systems are lamellar, hexagonal, and gyroid phases of CO_2-7(4) at hydration levels λ = 6.1, 12.9, and 12.9, respectively. The remaining three systems employ sulfonate headgroups, all at hydration level λ = 12.9 and are composed of surfactants SO_3-13(4), SO_3-7(4), and SO_3-7(4) for the lamellar, hexagonal, and gyroid phases, respectively. The composition and unit cells of these 11 systems are detailed in Table 1. We refer the reader to the work of Sorenson et al. for a discussion of the topology of the hexagonal, gyroid, and lamellar LLC morphologies.[6]

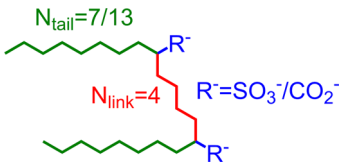

Figure 1. Gemini-surfactants utilized in this work. For example, nomenclature SO_3-13(4) denotes a gemini surfactant with sulfonate headgroups, 13 carbon atoms constituting each tail, and four linker carbon atoms.

The LLCs are constructed using MD simulations. The gyroid phase of CO_2-7(4) is taken from the previous work of Mondal et al.,[49] and the lamellar phase of CO_2-7(4) is taken from the previous work of McDaniel et al.[51] The CO_2-7(4) hexagonal phase and CO_2-13(4) lamellar phases are self-assembled utilizing appropriately chosen unit cells (*vide infra*). After self-assembling the first CO_2-13(4) lamellar phase, structures at additional hydration levels are formed by expanding or contracting the unit cell, adding or removing water molecules, and subsequent reequilibration. All sulfonate-surfactant morphologies are created from the corresponding carboxylate-surfactant morphologies by replacing the headgroups and then reequilibrating the systems.

MD simulations are conducted using the GROMACs-4.5 software package.[52] The NPT ensemble is used for equilibration, employing isotropic pressure coupling for the gyroid phases and semi-isotropic pressure coupling for the lamellar and hexagonal phases, utilizing the Berendsen barostat[53] and Nose−Hoover thermostat;[54,55] all simulations are at 300 K and 1 bar. The particle mesh Ewald (PME) algorithm[56] is used for electrostatics, and long-range van der Waals (VDW) interactions are cutoff at 1.4 nm. Equilibration times range from 50 to 500 ns, as determined by convergence of characteristic peaks of the structure factors, verifying LLC phase formation (*vide infra*). After equilibration, 100 ns NVT simulations are used for property characterization. All simulations employ the GROMOS force field[57] for the surfactant and sodium ions, in conjunction with the SPC model[58] for water. Charges for the surfactant headgroups were determined based on quantum mechanical calculations, with values of q_C = 0.27, q_O = −0.635 for carboxylate and q_S = 0.905, q_O = −0.635 for sulfonate. Structure factors are computed using β-spline interpolation followed by discrete Fourier transform (DFT), as is done in the PME approach[56] and described in the recent work of Mantha et al.[59]

To characterize the water dynamics, we compute translational self-diffusion coefficients and rotational correlation functions. Diffusion coefficients are calculated by

$$D_{H_2O} = \lim_{t\to\infty} \frac{1}{6} \frac{\partial \langle |\vec{r}_{H_2O}(t) - \vec{r}_{H_2O}(0)|^2 \rangle}{\partial t} \quad (1)$$

The rotational correlation function is calculated for the molecular axis z_{H_2O}, which is the unit vector perpendicular to the H−O−H water plane. The characteristic rotational relaxation time, τ_1, is defined as the integral of the rotational correlation function,

$$\tau_1 = \int_0^\infty dt \, \langle z_{H_2O}(t) \cdot z_{H_2O}(0) \rangle \quad (2)$$

3. RESULTS

3.1. Stability Considerations. We are able to create *in silico* morphologies that are not accessible in experiment by exploiting the small free energy differences between morphologies. Recent work by Mantha et al.[59] has suggested that different gemini surfactant-based LLC phases may be separated by very small free energy differences over a range of hydration levels. In practice, this means that LLC phases that are not observed experimentally may be metastable in computer simulations that involve finite systems and finite time scales. Additionally, standard simulations in the NPT ensemble utilizing either isotropic or semi-isotropic pressure coupling introduce a constraint on the LLC periodicity based on the choice of simulation box. For example, a hexagonal simulation box may bias formation of hexagonally packed cylinders due to

DOI: 10.1021/acs.jpcb.6b08087
J. Phys. Chem. B 2016, 120, 10860−10868

Table 1. Composition of Different Gemini Surfactant Systems

			number of molecules			
surfactant	phase	λ	surfactant	sodium	water	unit cell[a]
CO_2-7(4)	lamellar	6.1	100	200	614	4.51,4.28[b]
CO_2-13(4)	lamellar	6.1	134	268	823	7.28,3.03
CO_2-13(4)	lamellar	10.0	134	268	1340	7.59,3.01
CO_2-13(4)	lamellar	12.9	134	268	1729	7.84,2.99
CO_2-7(4)	hexagonal	12.9	24	48	310	3.18,2.84
CO_2-7(4)	gyroid	12.9	250	500	3225	6.40
SO_3-13(4)	lamellar	12.9	134	268	1729	7.91,3.02
SO_3-7(4)	hexagonal	12.9	24	48	310	3.22,2.88
SO_3-7(4)	gyroid	12.9	250	500	3225	6.49
CO_2-13(4)	lamellar	13.9	134	268	1863	7.95,2.99
CO_2-13(4)	lamellar	18.0	134	268	2412	8.04,3.15

[a]Unit cell parameters are given as follows (length in nm): the gyroid phase has a cubic unit cell, specified by a single length; the lamellar phase has a tetragonal unit cell, specified by length $a = b$, and perpendicular length c; the hexagonal phase is specified by the length of the a and b unit cell vectors (forming the 60° hexagonal angle), and the length of perpendicular vector c. We note that the $a = b$ lengths of the lamellar phases and the c length of the hexagonal phase are arbitrary since they are determined by the number of surfactant molecules in the system. [b]This cell contains two lamellar bilayers so that a longer VDW cutoff can be employed.

the periodicity constraint, even if a different phase exhibits lower free energy in the absence of this constraint. Free energy differences between LLC phases may be within the simulation uncertainty,[59] and predicting the lowest free energy LLC phase is therefore a highly difficult task; this is an important challenge for future research.

In this work, we have exploited these small free energy differences to assemble a variety of LLCs that are stable over the time scales accessible to the MD simulations. Some of these phases are not experimentally accessible: The hexagonal phase of CO_2-7(4) at $\lambda = 12.9$ is only observed experimentally at higher water content,[6] and the SO_3-7(4) gyroid phase is not observed experimentally with sodium counterions.[60] However, in lieu of explicit free energy calculations, there is no indication of instability throughout the simulation; the structure factors characterizing the long-range order (Figure 2) are converged and stable over hundreds of nanoseconds. Additionally, the potential energy density of the CO_2-7(4) hexagonal and gyroid phases at $\lambda = 12.9$ is within ~1% (with the hexagonal phase actually lower in energy), and previous work indicates similar entropy of these phases.[59] Additionally, we compare the energy density of the carboxylate and sulfonate LLC phases at $\lambda = 12.9$ hydration level; the ratio of energy densities is 1.09, 1.09, and 1.07 for the hexagonal, gyroid, and lamellar phases, respectively (with carboxylate LLCs exhibiting more negative energy densities), indicating no obvious destabilization of the gyroid phase with sulfonate headgroups, as is observed experimentally.

3.2. Structure Characterization. A comprehensive characterization of the structure of LLCs entails analysis of both the long-range liquid-crystalline periodic order and the short-range atomic pairwise correlation. The former is characterized by the intensity of low-q peaks in the structure factor, $S(q)$, that correspond to the periodicity of the crystal's reciprocal lattice. Short-range correlation is characterized through standard radial distribution functions.

The structure factors of the six different LLCs at hydration level $\lambda = 12.9$ are shown in Figure 2, along with corresponding representative snapshots from the simulation. The structure factors verify the long-range order of each different morphology (hexagonal, gyroid, lamellar), exhibiting scattering signatures nearly identical to corresponding experimental X-ray diffraction patterns.[6] In Figure 2, we have labeled each prominent scattering peak by its corresponding reciprocal lattice vector; the lamellar and hexagonal phases are 1D and 2D periodic, as all prominent scattering lattice vectors are in-plane, whereas the gyroid phase is a bicontinuous, 3D periodic structure evidenced by scattering at noncoplanar, higher index reciprocal lattice vectors. We note that both the carboxylate and sulfonate surfactant systems have similar structure factors for each LLC morphology, indicating that the LLC phases are not significantly perturbed by the different headgroups over the simulation time scales.

For brevity, we do not show structure factors of the CO_2-13(4) lamellar phases at hydration levels other than $\lambda = 12.9$ (we note that the CO_2-7(4), $\lambda = 6.1$ lamellar phase was characterized in ref 51). These additional lamellar phases exhibit similarly well-defined periodicity as the lamellar phase shown in Figure 2, but there is an interesting structural trend with hydration level. As shown in Table 1, the magnitude of the c unit cell vector, defining the thickness of one surfactant bilayer and one aqueous layer, does not increase with hydration level at low water content; rather the a and b vectors, which are tangential to the lamellar plane, increase in magnitude to accommodate the additional water molecules. Because the number of surfactant molecules is the same in all systems and the density of the bilayer is relatively constant, this means that the surfactant bilayer contracts (expands) perpendicular (parallel) to the lamellar plane with increasing hydration level (simulation snapshots are shown in the Supporting Information). This expansion/contraction of the bilayer occurs until a threshold hydration level between $\lambda = 14-18$, at which point expansion of the bilayer in the a and b directions ceases, and the additional water molecules are accommodated by increased interbilayer thickness (c); these changes in the relative bilayer dimensions correspondingly affect the surface density of headgroups and exposed hydrophobic area. We note that a similar phenomenon has been observed for certain biological lipid bilayers.[61,62]

The short-range, pairwise correlation between headgroups/water and headgroups/sodium are shown in Figure 3 for both carboxylate and sulfonate LLCs at $\lambda = 12.9$. Rather than plotting the radial distribution function, $g(r)$, we plot the pairwise probability density for finding a second atom type at a given distance from a "tagged" atom at the origin, defined as

DOI: 10.1021/acs.jpcb.6b08087
J. Phys. Chem. B 2016, 120, 10860−10868

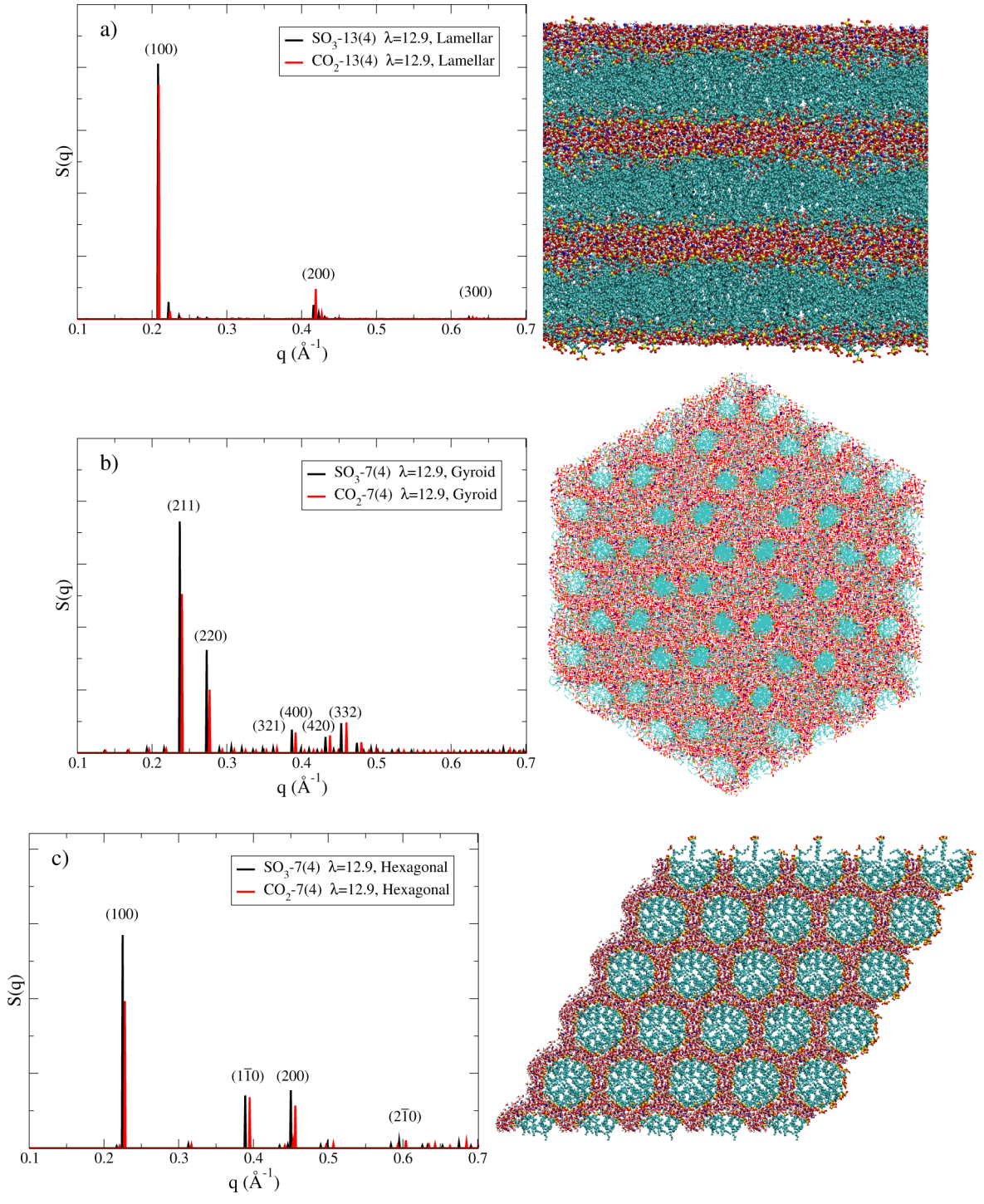

Figure 2. Structure factors and corresponding simulation snapshots for LLC morphologies at λ = 12.9 hydration: (a) lamellar, (b) gyroid, and (c) hexagonal morphologies. Structure factors are shown for both carboxylate and sulfonate based surfactants, whereas the snapshots depict only the sulfonate surfactant systems. Atom types are colored as follows: H, white; Na, blue; C, cyan; O, red, S, yellow.

$\rho_2 \cdot g_{12}(r)$, where ρ_2 is the density of the second atom type (nm^{-3}). This is the appropriate metric for comparison, because the lamellar systems have different water, sodium, and headgroup densities due to the longer surfactant tails. For each system, we plot the correlation between the oxygen atoms of the headgroup and either sodium or hydrogen (water) atoms.

For a specific headgroup (e.g., carboxylate), the headgroup/sodium correlation shows a small dependence on system morphology, while the headgroup/water correlation is very nearly independent of morphology. The morphology dependence of the headgroup/sodium distribution can be understood as follows: Recently, Mantha et al.[59] showed that the headgroup/counterion correlation is largely dictated by the required screening to stabilize the headgroup/headgroup repulsion; namely, greater headgroup/headgroup repulsion leads to greater headgroup/counterion correlation. In general, the headgroup/headgroup repulsion should decrease with

DOI: 10.1021/acs.jpcb.6b08087
J. Phys. Chem. B 2016, 120, 10860−10868

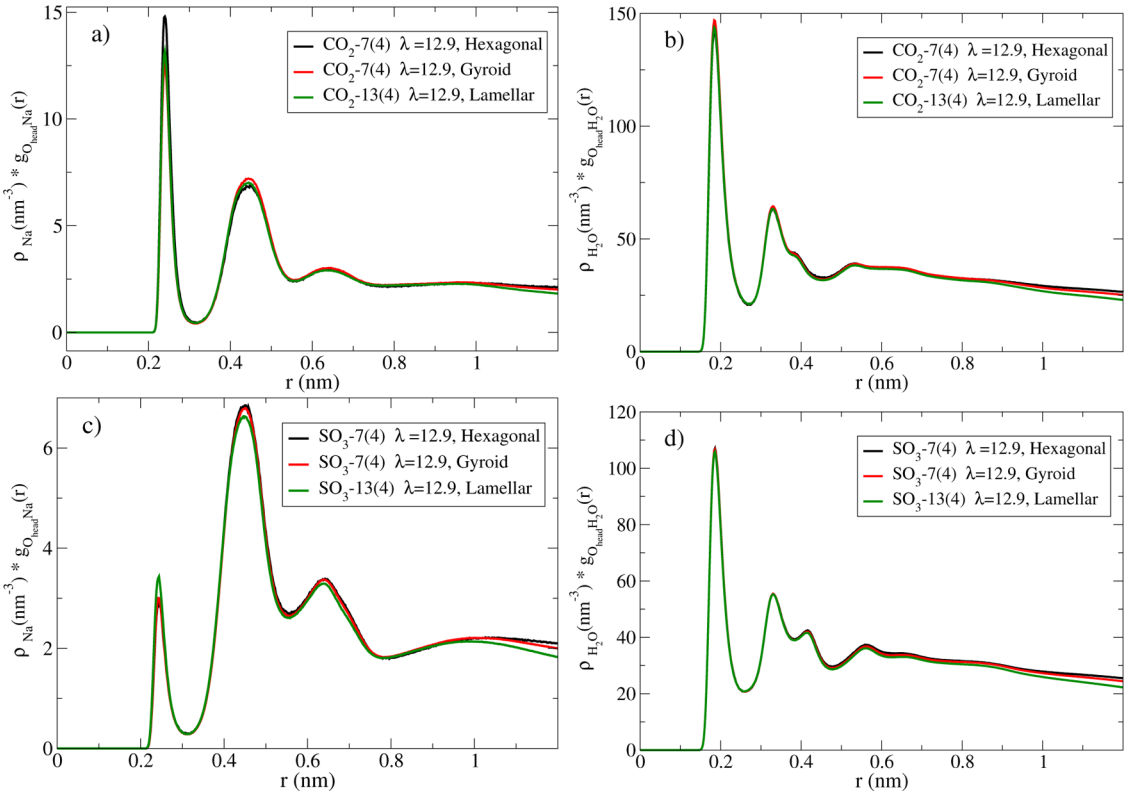

Figure 3. Pairwise probability distributions for carboxylate LLCs: (a) headgroup/sodium; (b) headgroup/water and sulfonate LLCs; (c) headgroup/sodium; (d) headgroup/water. In all cases, the pairwise probability is computed between the oxygen atoms of the headgroup and either sodium or hydrogen (water) atoms. To normalize for systems of different density, we plot $\rho \cdot g(r)$ rather than $g(r)$.

increasing curvature of the interface, in the order lamellar > gyroid > hexagonal.[59] This explains why the headgroup/sodium correlation is slightly higher for lamellar compared to gyroid phases for both types of headgroups. For the hexagonal phase, there are two contrasting effects, namely, intercylinder headgroup/headgroup repulsion and intracylinder headgroup/headgroup repulsion. For LLCs at higher hydration,[59] the intercylinder distance is larger, reducing repulsion between cylinders, and the hexagonal phase thus exhibits lower headgroup/sodium correlation compared to the gyroid due to the enhanced curvature of the surfactant/water interface. The LLCs in this work are at lower hydration, λ = 12.9, bringing the cylinders in the hexagonal phase closer together, increasing the headgroup/headgroup repulsion between cylinders, and leading to higher headgroup/sodium correlation in the hexagonal compared to gyroid phase for carboxylate surfactants (Figure 3a). For the sulfonate surfactant systems at λ = 12.9, the reduction in electrostatics due to the sulfonate headgroup alters this balance, and the gyroid and hexagonal phases exhibit similar headgroup/sodium correlation (Figure 3c).

3.3. Dynamics. The focus of this work is characterizing the dynamics of water in LLC nanoconfined systems. We have confirmed the LLC periodicity of the hexagonal, gyroid, and lamellar phases (section 3.2), and we now systematically evaluate the influence of morphology, surfactant functionality, and hydration level on the water dynamics.

Rotational correlation functions of water are computed for each LLC and are shown in Figure 4. Although the 11 LLCs differ in morphology and nature of surfactant, to a good approximation the rotational dynamics of water primarily depends on the hydration level. To emphasize this, the data in

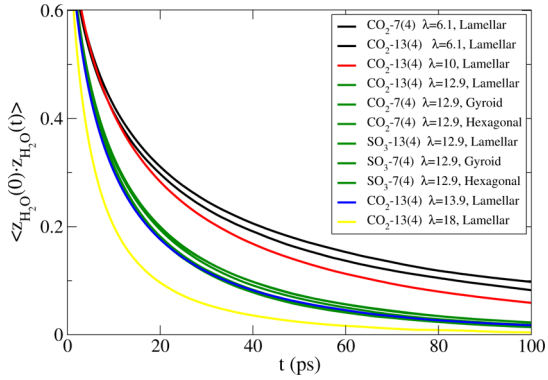

Figure 4. Rotational correlation function for water in LLC morphologies at 300 K: z_{H_2O} is the vector perpendicular to the H−O−H plane of the water molecule. Systems are colored according to their hydration level with λ = 6.1 black curves, λ = 10 red curves, λ = 12.9 green curves, λ = 13.9 blue curves, and λ = 18 yellow curves.

Figure 4 is color-coded according to the hydration level of each LLC: From lowest to highest hydration, λ = 6.1 (black), λ = 10 (red), λ = 12.9 (green), λ = 13.9 (blue), and λ = 18 (yellow). It is obvious that the dynamics is highly dependent on water content, with the most hydrated LLC, λ = 18 (yellow), exhibiting significantly faster dynamics than the least hydrated LLC(s), λ = 6.1 (black). The fact that the rotational correlation functions are well-grouped according to color (hydration level) indicates that differences in the morphology and chemical functionality of the LLCs are significantly less influential on the water dynamics than is the hydration level.

DOI: 10.1021/acs.jpcb.6b08087
J. Phys. Chem. B 2016, 120, 10860−10868

To quantify the dynamic time scales, the rotational correlation functions are integrated to give characteristic rotational relaxation times, τ_1 (eq 2). In Figure 5, we plot τ_1 versus hydration level, λ, for each LLC; as a reference, $\tau_1 \approx 3$ ps as computed with the SPC model for bulk water at 298 K.[63] For all LLC systems, rotational relaxation times are significantly longer, with $\tau_1 \approx 2-3$ times larger for the most hydrated system ($\lambda = 18$) compared to bulk water (convergence to the bulk value should not be expected due to the presence of ions[11,64]). The dashed line in Figure 5 is an exponential fit to the hydration dependence of τ_1 for the CO_2-13(4) lamellar systems: It is clear that the τ_1 relaxation times for all LLCs only exhibit small deviations from this "general" hydration dependent trend. While these conclusions are based on the integrated time τ_1, a corresponding analysis of biexponential fits to the rotational correlation functions gives an analogous qualitative interpretation (Supporting Information).

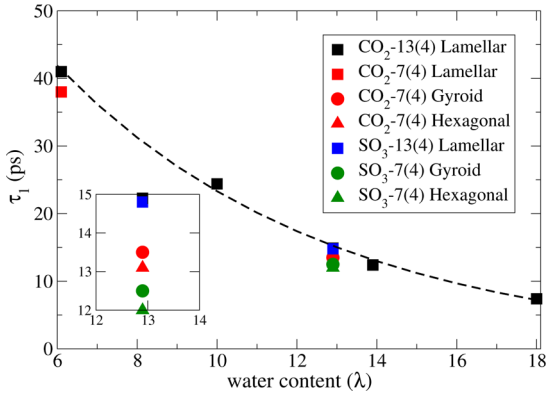

Figure 5. Rotational correlation time τ_1 for water in LLC morphologies at 300 K. The symbol shape denotes morphology (■, lamellar; ●, gyroid; ▲, hexagonal) and color denotes surfactant type (black, CO_2-13(4); red, CO_2-7(4); blue, SO_3-13(4); green, SO_3-7(4)). The dashed line is an exponential fit to the data of the CO_2-13(4) lamellar systems and is to guide the eye. The inset is a blowup of the $\lambda = 12.9$ region.

We now analyze the influence of different morphologies and surfactant functionality on the water dynamics, keeping in mind that these effects are largely secondary to hydration level; because of this, such a comparison is only justified across LLCs at constant λ, which is enabled by the systems studied in this work. For clarity, we show an enlarged inset in Figure 5 of the six LLC systems at $\lambda = 12.9$. For both sulfonate- and carboxylate-based surfactants, the water dynamics is somewhat affected by the LLC morphology, with dynamical rates decreasing in order hexagonal > gyroid > lamellar. It is important to note that the lamellar phases at $\lambda = 12.9$ employ longer tail surfactants (13) compared to the gyroid and hexagonal phases (7), which also affects the dynamics (*vide infra*), and thus the effect of morphology is not entirely isolated in this case. Differences in the water dynamics among morphologies may be due to differences in the interfacial curvature of the hexagonal, gyroid, and lamellar LLCs. In a previous work, Pieniazek et al.[25] established a "curvature-induced frustration" effect for water dynamics in reverse micelles. These authors showed that the distance over which water molecules were affected by the surface depended on the curvature of the interface; dynamics slows most for highly concave interfaces, such as in small reverse micelles. Relatedly, convex interfaces may exhibit enhanced water dynamics compared to flat interfaces.[31] Our results are consistent with this interpretation; water dynamics is fastest in the morphology with convex curvature (hexagonal), followed by mixed curvature (gyroid), followed by flat interfaces (lamellar). It is important to note, however, that the quantitative extent of these curvature effects is much smaller than previously suggested.[31]

The nature of the surfactant headgroup has a (relatively) small effect on the water dynamics. For the six LLC systems at $\lambda = 12.9$, Figure 5 shows that the rotational relaxation of water is slightly faster for sulfonate compared to carboxylate surfactants for a given morphology. This is presumably due to the strength of the headgroup/water interaction; in Figure 3, it was shown that both headgroup/sodium and headgroup/water interactions are weaker for the oxygen atoms of sulfonate compared to carboxylate headgroups. These weaker interactions lead to faster water rearrangement, consistent with the smaller rotational correlation times (τ_1) in sulfonate systems. Besides the headgroup, the length of the surfactant tail also affects the water dynamics, for example, the CO_2-13(4) lamellar system exhibits slower water dynamics compared to the CO_2-7(4) lamellar system, both at $\lambda = 6.1$. The reason for this is more subtle, but we propose that this is due to the mobility of the hydrophobic surfactant layer, and the influence of surfactant motion on the interfacial water dynamics; the longer tailed surfactant phase is less mobile, decreasing the water dynamics. We also partially attribute the difference in water dynamics of the lamellar and gyroid systems at $\lambda = 12.9$ to this effect.

The self-diffusion coefficients provide a complementary analysis of the water dynamics; they pertain to significantly longer (nanosecond) time scales and translational dynamics, as opposed to the rotational relaxation time. In Figure 6, we plot the water MSD versus time in each LLC, and as before the data is color-coded according to hydration level. Dynamic trends are similar to the rotational correlation functions (Figure 4), and it is again seen that hydration level is the dominate factor influencing the dynamics. However, differences between systems are somewhat more pronounced in this metric, and indeed the resulting diffusion coefficients vary over an order of magnitude (Figure 7).

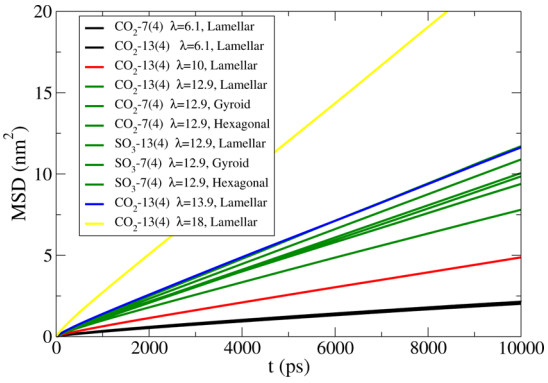

Figure 6. Mean square displacement (MSD) of water in LLC morphologies at 300 K. Systems are colored according to their hydration level, with $\lambda = 6.1$ (black), $\lambda = 10$ (red), $\lambda = 12.9$ (green), $\lambda = 13.9$ (blue), and $\lambda = 18$ (yellow).

Corresponding diffusion coefficients are shown in Figure 7 as a function of hydration level; similar to Figure 5, symbols and colors are chosen to distinguish the surfactant type and

DOI: 10.1021/acs.jpcb.6b08087
J. Phys. Chem. B 2016, 120, 10860−10868

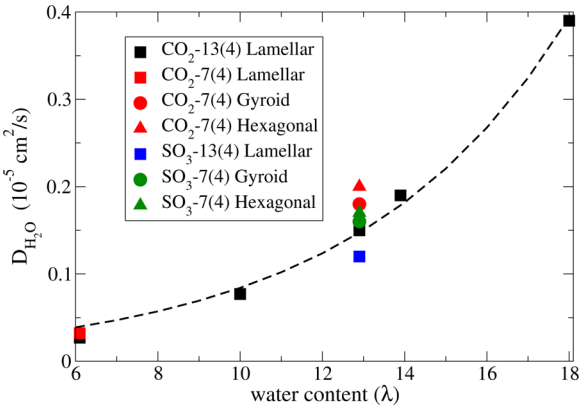

Figure 7. Water self-diffusion coefficient in LLC morphologies at 300 K. Data for systems composed of the same surfactant are plotted as same color, while data for systems of the same morphology are plotted as same shape, analogous to Figure 5. The dashed line is an exponential fit to the data of the CO_2-13(4) lamellar systems and is to guide the eye.

morphology of the LLC. As a reference, the diffusion coefficient of bulk water at 298 K as predicted by the SPC model is $\sim 4 \cdot 10^{-5}$ $cm^2 s^{-1}$,[63] and for all the LLC systems, the water diffusion coefficient is at least an order of magnitude smaller. The translational dynamics mostly follow the same qualitative trends as discussed in the analysis of rotational correlation times; interestingly, however, there is one important exception: *The trend in water dynamics upon substitution of different surfactant headgroups is opposite for the self-diffusion coefficients* (Figure 7) *from that of the rotational correlation times* (Figure 5). Water diffusion is slower for sulfonate compared to carboxylate LLCs, whereas the rotational relaxation is faster (smaller τ_1) for sulfonate-based systems. This seemingly nonintuitive result may be understood by more thoroughly considering the headgroup/water pairwise distributions in Figure 3b,d. While there is less correlation between each headgroup oxygen atom and water for sulfonate, there are three to two such headgroup oxygen atoms for sulfonate compared to carboxylate. This means that the sulfonate headgroup effectively binds more water molecules compared to carboxylate (this was verified by computing the total headgroup/water correlation, not shown, and is explained by the highly structured solvation shell of sulfonate anions[65]). Thus, the explanation for the headgroup dependent data of Figure 7 and Figure 5 is that the sulfonate headgroup binds more water molecules than carboxylate but each is bound more weakly.

4. DISCUSSION/CONCLUSION

Due to the ubiquity of chemical and biological systems that contain water in various states of nanoconfinement, the physics of confined water has been heavily studied both experimentally and theoretically, as evidenced by numerous review articles.[1−3,8,22,30,33,66] Contributing to this discussion therefore requires care, both to not reiterate previous findings and to appropriately present new work in a contextual manner. Thus, we have largely avoided analysis of the physical mechanisms by which water moves and reorients and how these mechanisms are affected by ions, interfaces, and confinement; such an analysis may be found in the many excellent works that have been cited. Rather, the primary contribution of this work is the comprehensive quantitative characterization of dynamics for a novel collection of gemini surfactant-based LLCs, which we believe has allowed for unprecedented systematic isolation of the different effects of confinement, morphology, and chemical functionality on water dynamics. The results of this study are an important quantitative benchmark for a novel class of systems, to which previous theories of water dynamics in confinement may be evaluated.

We have shown that gemini surfactant-based LLCs are ideal prototypical systems for systematically studying water dynamics in confinement. The variety of morphologies (hexagonal, gyroid, lamellar) allows characterization of the influence of interfacial curvature, water channel topology, and long-range, periodic order. Furthermore, the liquid-crystalline nature enables unambiguous structural characterization, so that the topologies and length scales of these systems are well-defined. While reverse micelles have served as popular prototypical systems for studying water dynamics in confinement, the dimensionality of confinement (3D) renders generalization difficult to many other practical systems (with 2D confinement). Quantifying the effect of one parameter, for example, interfacial curvature, on the resulting water dynamics is best done when other variables (dimensionality, chemical functionality, hydration level, etc.) are held constant, as we have demonstrated for gemini surfactant-based LLCs.

Our primary qualitative conclusion is that the hydration level of nanoconfined systems predominately determines the rates of water dynamics, and that other variables such as interfacial curvature, chemical functionality, and topology are secondary in importance. This was demonstrated through analysis of 11 different gemini surfactant-based LLCs, considering two distinct dynamical metrics. This conclusion is important in light of conflicting interpretations in the literature,[18,31] as well as for the novelty of the systems studied. Secondary effects may differentiate systems at identical hydration level, and our finding that rates of water dynamics depend on morphology in order hexagonal > gyroid > lamellar is consistent with previous work[25,31] that suggests that convex surfaces enhance dynamics compared to flat or concave interfaces. Additionally, we suggest that water dynamics may be coupled to the mobility of the surfactant lipid phase, since these dynamics are faster in shorter-tail (and thus presumably more mobile) surfactant-based LLCs. All of these conclusions are strengthened by the explicit isolation of confinement parameters that is achieved in this work.

Finally, we have illustrated the importance of analyzing different metrics of dynamics that encompass a range of time scales. We have shown that substituting sulfonate for carboxylate headgroups has contrasting effects on the rates of rotational relaxation and translational diffusion of confined water. Sulfonate headgroups effectively bind more water molecules than carboxylate, resulting in slower net translational diffusion of water, but each water molecule is bound less strongly, which results in faster rotational relaxation. A complete dynamical picture is not possible without both metrics, and the relative importance of these two processes may depend on the specific application.

■ ASSOCIATED CONTENT

Supporting Information

The Supporting Information is available free of charge on the ACS Publications website at DOI: 10.1021/acs.jpcb.6b08087.

Simulation snapshots of CO_2-13(4) lamellar phases at different hydration levels, biexponential analysis of

DOI: 10.1021/acs.jpcb.6b08087
J. Phys. Chem. B 2016, 120, 10860−10868

rotational correlation functions, and correlation function for water/headgroup close-contacts (PDF)

AUTHOR INFORMATION

Corresponding Author

*E-mail: yethiraj@chem.wisc.edu. Phone: +1 (608) 262-0258.

Notes

The authors declare no competing financial interest.

ACKNOWLEDGMENTS

This research is supported by Department of Energy, Basic Energy Sciences, through Grant DE-SC0010328. Computational resources were provided by the Center for High Throughput Computing at the University of Wisconsin. The CHTC is supported by UW-Madison, the Advanced Computing Initiative, the Wisconsin Alumni Research Foundation, the Wisconsin Institutes for Discovery, and the National Science Foundation and is an active member of the Open Science Grid, which is supported by the National Science Foundation and the U.S. Department of Energy's Office of Science. This research was supported in part by National Science Foundation Grant CHE-0840494.

REFERENCES

(1) Berkowitz, M. L.; Vacha, R. Aqueous Solutions at the Interface with Phospholipid Bilayers. *Acc. Chem. Res.* **2012**, *45*, 74−82.

(2) Fayer, M. D.; Levinger, N. E. Analysis of Water in Confined Geometries and at Interfaces. *Annu. Rev. Anal. Chem.* **2010**, *3*, 89−107.

(3) Rasaiah, J. C.; Garde, S.; Hummer, G. Water in Nonpolar Confinement: From Nanotubes to Proteins and Beyond. *Annu. Rev. Phys. Chem.* **2008**, *59*, 713−740.

(4) Bourg, I. C.; Steefel, C. I. Molecular Dynamics Simulations of Water Structure and Diffusion in Silica Nanopores. *J. Phys. Chem. C* **2012**, *116*, 11556−11564.

(5) Mauritz, K. A.; Moore, R. B. State of Understanding of Nafion. *Chem. Rev.* **2004**, *104*, 4535−4586.

(6) Sorenson, G. P.; Coppage, K. L.; Mahanthappa, M. K. Unusually Stable Aqueous Lyotropic Gyroid Phases from Gemini Dicarboxylate Surfactants. *J. Am. Chem. Soc.* **2011**, *133*, 14928−14931.

(7) Bhattacharyya, K.; Bagchi, B. Slow Dynamics of Constrained Water in Complex Geometries. *J. Phys. Chem. A* **2000**, *104*, 10603−10613.

(8) Nandi, N.; Bhattacharyya, K.; Bagchi, B. Dielectric Relaxation and Solvation Dynamics of Water in Complex Chemical and Biological Systems. *Chem. Rev.* **2000**, *100*, 2013−2046.

(9) Dokter, A. M.; Woutersen, S.; Bakker, H. J. Anomalous Slowing Down of the Vibrational Relaxation of Liquid Water upon Nanoscale Confinement. *Phys. Rev. Lett.* **2005**, *94*, 178301.

(10) Dokter, A. M.; Woutersen, S.; Bakker, H. J. Inhomogeneous Dynamics in Confined Water Nanodroplets. *Proc. Natl. Acad. Sci. U. S. A.* **2006**, *103*, 15355−15358.

(11) Dokter, A. M.; Woutersen, S.; Bakker, H. J. Ultrafast Dynamics of Water in Cationic Micelles. *J. Chem. Phys.* **2007**, *126*, 124507.

(12) Cringus, D.; Bakulin, A.; Lindner, J.; Vohringer, P.; Pshenichnikov, M. S.; Wiersma, D. A. Ultrafast Energy Transfer in Water-AOT Reverse Micelles. *J. Phys. Chem. B* **2007**, *111*, 14193−14207.

(13) Tan, H.-S.; Piletic, I. R.; Riter, R. E.; Levinger, N. E.; Fayer, M. D. Dynamics of Water Confined on a Nanometer Length Scale in Reverse Micelles: Ultrafast Infrared Vibrational Echo Spectroscopy. *Phys. Rev. Lett.* **2005**, *94*, 057405.

(14) Piletic, I. R.; Moilanen, D. E.; Spry, D. B.; Levinger, N. E.; Fayer, M. D. Testing the Core/Shell Model of Nanoconfined Water in Reverse Micelles Using Linear and Nonlinear IR Spectroscopy. *J. Phys. Chem. A* **2006**, *110*, 4985−4999.

(15) Zhao, W.; Moilanen, D. E.; Fenn, E. E.; Fayer, M. D. Water at the Surfaces of Aligned Phospholipid Multibilayer Model Membranes Probed with Ultrafast Vibrational Spectroscopy. *J. Am. Chem. Soc.* **2008**, *130*, 13927−13937.

(16) Park, S.; Moilanen, D. E.; Fayer, M. D. Water Dynamics-The Effects of Ions and Nanoconfinement. *J. Phys. Chem. B* **2008**, *112*, 5279−5290.

(17) Moilanen, D. E.; Levinger, N. E.; Spry, D. B.; Fayer, M. D. Confinement or the Nature of the Interface? Dynamics of Nanoscopic Water. *J. Am. Chem. Soc.* **2007**, *129*, 14311−14318.

(18) Moilanen, D. E.; Fenn, E. E.; Wong, D.; Fayer, M. D. Geometry and Nanolength Scales versus Interface Interactions: Water Dynamics in AOT Lamellar Structures and Reverse Micelles. *J. Am. Chem. Soc.* **2009**, *131*, 8318−8328.

(19) Moilanen, D. E.; Fenn, E. E.; Wong, D.; Fayer, M. D. Water Dynamics in Large and Small Reverse Micelles: From Two Ensembles to Collective Behavior. *J. Chem. Phys.* **2009**, *131*, 014704.

(20) Fenn, E. E.; Wong, D. B.; Fayer, M. D. Water Dynamics at Neutral and Ionic Interfaces. *Proc. Natl. Acad. Sci. U. S. A.* **2009**, *106*, 15243−15248.

(21) Fenn, E. E.; Wong, D. B.; Giammanco, C. H.; Fayer, M. D. Dynamics of Water at the Interface in Reverse Micelles: Measurements of Spectral Diffusion with Two-Dimensional Infrared Vibrational Echoes. *J. Phys. Chem. B* **2011**, *115*, 11658−11670.

(22) Fayer, M. D. Dynamics of Water Interacting with Interfaces, Molecules, and Ions. *Acc. Chem. Res.* **2012**, *45*, 3−14.

(23) Faeder, J.; Ladanyi, B. M. Molecular Dynamics Simulations of the Interior of Aqueous Reverse Micelles. *J. Phys. Chem. B* **2000**, *104*, 1033−1046.

(24) Zhang, Z.; Berkowitz, M. L. Orientational Dynamics of Water in Phospholipid Bilayers with Different Hydration Levels. *J. Phys. Chem. B* **2009**, *113*, 7676−7680.

(25) Pieniazek, P. A.; Lin, Y.-S.; Chowdhary, J.; Ladanyi, B. M.; Skinner, J. L. Vibrational Spectroscopy and Dynamics of Water Confined inside Reverse Micelles. *J. Phys. Chem. B* **2009**, *113*, 15017−15028.

(26) Gruenbaum, S. M.; Skinner, J. L. Vibrational Spectroscopy of Water in Hydrated Lipid Multi-Bilayers. I. Infrared Spectra and Ultrafast Pump-Probe Observables. *J. Chem. Phys.* **2011**, *135*, 075101.

(27) Gruenbaum, S. M.; Pieniazek, P. A.; Skinner, J. L. Vibrational Spectroscopy of Water in Hydrated Lipid Multi-Bilayers. II. Two-Dimensional Infrared and Peak Shift Observables Within Different Theoretical Approximations. *J. Chem. Phys.* **2011**, *135*, 164506.

(28) Gruenbaum, S. M.; Skinner, J. L. Vibrational Spectroscopy of Water in Hydrated Lipid Multi-Bilayers. III. Water Clustering and Vibrational Energy Transfer. *J. Chem. Phys.* **2013**, *139*, 175103.

(29) Bakulin, A. A.; Cringus, D.; Pieniazek, P. A.; Skinner, J. L.; Jansen, T. L. C.; Pshenichnikov, M. S. Dynamics of Water Confined in Reversed Micelles: Multidimensional Vibrational Spectroscopy Study. *J. Phys. Chem. B* **2013**, *117*, 15545−15558.

(30) Skinner, J. L.; Pieniazek, P. A.; Gruenbaum, S. M. Vibrational Spectroscopy of Water at Interfaces. *Acc. Chem. Res.* **2012**, *45*, 93−100.

(31) Roy, S.; Skoff, D.; Perroni, D. V.; Mondal, J.; Yethiraj, A.; Mahanthappa, M.; Zanni, M.; Skinner, J. L. Water Dynamics in Gyroid Phases of Self-Assembled Gemini Surfactants. *J. Am. Chem. Soc.* **2016**, *138*, 2472−2475.

(32) Nihonyanagi, S.; Yamaguchi, S.; Tahara, T. Direct Evidence for Orientational Flip-Flop of Water Molecules at Charged Interfaces: A Heterodyne-Detected Vibrational Sum Frequency Generation Study. *J. Chem. Phys.* **2009**, *130*, 204704.

(33) Nihonyanagi, S.; Mondal, J. A.; Yamaguchi, S.; Tahara, T. Structure and Dynamics of Interfacial Water Studied by Heterodyne-Detected Vibrational Sum-Frequency Generation. *Annu. Rev. Phys. Chem.* **2013**, *64*, 579−603.

(34) Roy, S.; Gruenbaum, S. M.; Skinner, J. L. Theoretical Vibrational Sum-Frequency Generation Spectroscopy of Water Near Lipid and Surfactant Monolayer Interfaces. *J. Chem. Phys.* **2014**, *141*, 18C502.

DOI: 10.1021/acs.jpcb.6b08087
J. Phys. Chem. B 2016, 120, 10860−10868

(35) Roy, S.; Gruenbaum, S. M.; Skinner, J. L. Theoretical Vibrational Sum-Frequency Generation Spectroscopy of Water Near Lipid and Surfactant Monolayer Interfaces. II. Two-Dimensional Spectra. *J. Chem. Phys.* **2014**, *141*, 22D505.
(36) Gilijamse, J. J.; Lock, A. J.; Bakker, H. J. Dynamics of Confined Water Molecules. *Proc. Natl. Acad. Sci. U. S. A.* **2005**, *102*, 3202−3207.
(37) Singh, P. C.; Nihonyanagi, S.; Yamaguchi, S.; Tahara, T. Ultrafast Vibrational Dynamics of Water at a Charged Interface Revealed by Two-Dimensional Heterodyne-Detected Vibrational Sum Frequency Generation. *J. Chem. Phys.* **2012**, *137*, 094706.
(38) Singh, P. C.; Nihonyanagi, S.; Yamaguchi, S.; Tahara, T. Communication: Ultrafast Vibrational Dynamics of Hydrogen Bond Network Terminated at the Air/Water Interface: A Two-Dimensional Heterodyne-Detected Vibrational Sum Frequency Generation Study. *J. Chem. Phys.* **2013**, *139*, 161101.
(39) Ni, Y.; Gruenbaum, S. M.; Skinner, J. L. Slow Hydrogen-Bond Switching Dynamics at the Water Surface Revealed by Theoretical Two-Dimensional Sum-Frequency Spectroscopy. *Proc. Natl. Acad. Sci. U. S. A.* **2013**, *110*, 1992−1998.
(40) Ni, Y.; Skinner, J. L. IR and SFG Vibrational Spectroscopy of the Water Bend in the Bulk Liquid and at the Liquid-Vapor Interface, Respectively. *J. Chem. Phys.* **2015**, *143*, 014502.
(41) Menger, F. M.; Littau, C. A. Gemini Surfactants: A New Class of Self-Assembling Molecules. *J. Am. Chem. Soc.* **1993**, *115*, 10083−10090.
(42) Menger, F. M.; Keiper, J. S. Gemini Surfactants. *Angew. Chem., Int. Ed.* **2000**, *39*, 1906−1920.
(43) Zana, R. Gemini (Dimeric) Surfactants. *Curr. Opin. Colloid Interface Sci.* **1996**, *1*, 566−571.
(44) Zana, R. Dimeric (Gemini) Surfactants: Effect of the Spacer Group on the Association Behavior in Aqueous Solution. *J. Colloid Interface Sci.* **2002**, *248*, 203−220.
(45) Pindzola, B. A.; Jin, J.; Gin, D. L. Cross-Linked Normal Hexagonal and Bicontinuous Cubic Assemblies via Polymerizable Gemini Amphiphiles. *J. Am. Chem. Soc.* **2003**, *125*, 2940−2949.
(46) Zhou, M.; Nemade, P. R.; Lu, X.; Zeng, X.; Hatakeyama, E. S.; Noble, R. D.; Gin, D. L. New Type of Membrane Material for Water Desalination Based on a Cross-Linked Bicontinuous Cubic Lyotropic Liquid Crystal Assembly. *J. Am. Chem. Soc.* **2007**, *129*, 9574−9575.
(47) Hatakeyama, E. S.; Wiesenauer, B. R.; Gabriel, C. J.; Noble, R. D.; Gin, D. L. Nanoporous, Bicontinuous Cubic Lyotropic Liquid Crystal Networks via Polymerizable Gemini Ammonium Surfactants. *Chem. Mater.* **2010**, *22*, 4525−4527.
(48) Perroni, D. V.; Baez-Cotto, C. M.; Sorenson, G. P.; Mahanthappa, M. K. Linker Length-Dependent Control of Gemini Surfactant Aqueous Lyotropic Gyroid Phase Stability. *J. Phys. Chem. Lett.* **2015**, *6*, 993−998.
(49) Mondal, J.; Mahanthappa, M.; Yethiraj, A. Self-Assembly of Gemini Surfactants: A Computer Simulation Study. *J. Phys. Chem. B* **2013**, *117*, 4254−4262.
(50) Mantha, S.; Yethiraj, A. Dynamics of Water Confined in Lyotropic Liquid Crystals: Molecular Dynamics Simulations of the Dynamic Structure Factor. *J. Chem. Phys.* **2016**, *144*, 084504.
(51) McDaniel, J. G.; Yethiraj, A. Importance of Hydrophobic Traps for Proton Diffusion in Lyotropic Liquid Crystals. *J. Chem. Phys.* **2016**, *144*, 094705.
(52) Pronk, S.; Pall, S.; Schulz, R.; Larsson, P.; Bjelkmar, P.; Apostolov, R.; Shirts, M. R.; Smith, J. C.; Kasson, P. M.; van der Spoel, D.; et al. GROMACS 4.5: A High-Throughput and Highly Parallel Open Source Molecular Simulation Toolkit. *Bioinformatics* **2013**, *29*, 845−854.
(53) Berendsen, H. J. C.; Postma, J. P. M.; van Gunsteren, W. F.; DiNola, A.; Haak, J. R. Molecular Dynamics with Coupling to an External Bath. *J. Chem. Phys.* **1984**, *81*, 3684−3690.
(54) Nose, S. A Molecular Dynamics Method for Simulations in the Canonical Ensemble. *Mol. Phys.* **1984**, *52*, 255−268.
(55) Hoover, W. G. Canonical Dynamics: Equilibrium Phase-Space Distributions. *Phys. Rev. A: At., Mol., Opt. Phys.* **1985**, *31*, 1695−1697.
(56) Essmann, U.; Perera, L.; Berkowitz, M. L.; Darden, T.; Lee, H.; Pedersen, L. G. A Smooth Particle Mesh Ewald Method. *J. Chem. Phys.* **1995**, *103*, 8577−8593.
(57) Schuler, L. D.; Daura, X.; van Gunsteren, W. F. An Improved GROMOS96 Force Field for Aliphatic Hydrocarbons in the Condensed Phase. *J. Comput. Chem.* **2001**, *22*, 1205−1218.
(58) Berendsen, H.; Postma, J.; van Gunsteren, W.; Hermans, J. In *Intermolecular Forces: Proceedings of the Fourteenth Jerusalem Symposium on Quantum Chemistry and Biochemistry*; Pullman, B., Ed.; D. Reidel: Dordrecht, the Netherlands, 1981; Vol. *14*; pp 331−342.
(59) Mantha, S.; McDaniel, J. G.; Perroni, D. V.; Mahanthappa, M. K.; Yethiraj, A. Electrostatic Interactions Govern "Odd-Even" Effects in Water-Induced Gemini Surfactant Self-assembly. *J. Phys. Chem. B* **2016**, submitted for publication.
(60) Mahanthappa, M. K. Private Communication.
(61) Hristova, K.; White, S. H. Determination of the Hydrocarbon Core Structure of Fluid Dioleoylphosphocholine (DOPC) Bilayers by X-Ray Diffraction Using Specific Bromination of the Double-Bonds: Effect of Hydration. *Biophys. J.* **1998**, *74*, 2419−2433.
(62) Mashl, R. J.; Scott, H. L.; Subramaniam, S.; Jakobsson, E. Molecular Simulation of Dioleoylphosphatidylcholine Lipid Bilayers at Differing Levels of Hydration. *Biophys. J.* **2001**, *81*, 3005−3015.
(63) Wu, Y.; Tepper, H. L.; Voth, G. A. Flexible Simple Point-Charge Water Model with Improved Liquid-State Properties. *J. Chem. Phys.* **2006**, *124*, 024503.
(64) Lin, Y.-S.; Auer, B. M.; Skinner, J. L. Water Structure, Dynamics, and Vibrational Spectroscopy in Sodium Bromide Solutions. *J. Chem. Phys.* **2009**, *131*, 144511.
(65) Wang, C.; Clark, J. K., II; Kumar, M.; Paddison, S. J. An Ab Initio Study of the Primary Hydration and Proton Transfer of CF3SO3H and CF3O(CF2)2SO3H: Effects of the Hybrid Functional and Inclusion of Diffuse Functions. *Solid State Ionics* **2011**, *199−200*, 6−13.
(66) Cerveny, S.; Mallamace, F.; Swenson, J.; Vogel, M.; Xu, L. Confined Water as Model of Supercooled Water. *Chem. Rev.* **2016**, *116*, 7608−7625.

DOI: 10.1021/acs.jpcb.6b08087
J. Phys. Chem. B 2016, 120, 10860−10868